Review

Optical Rectennas -A Review

Yuvam Bhateja *

Posted Date: 25 September 2024

doi: 10.20944/preprints202409.1932.v1

Keywords: Levelized Cost of Energy; Rectenna; Shockley-Quiesser limit; Metal-Double-Insulator-Metal diodes; CNT-Insulator-Metal diodes; Point-contact-Metal-Insulator-Metal diodes

 doi:10.20944/preprints202409.1932.v

Review

Optical Rectennas—A Review

Yuvam Bhateja

Department of Physics, Politecnico Di Milano, Milan, Italy; yuvam.bhateja@mail.polimi.it

Abstract: With the ever-growing geopolitical tensions across borders arising, ultimately from the eternal energy needs, it is the peak time for humanity to put its reliance on a more quasi-perpetuity source of energy, such as the Sun. Even though current photovoltaics are the frontier of solar power harvesting, their efficiencies are reaching a state of stasis sooner or later. The efficiencies of single-junction solar cells are capped by the Shockley-Quiesser limit of 33.7%. Researchers are racing toward a way to beat this limit while keeping the Levelized Cost of Energy (LCE) to its minimum. Amongst all contenders, rectenna (or rectifying antenna), which was invented only a decade after the first practical PV cell by the Bells lab [1], is the most promising technology to take the forefront in quenching the energy needs, not only because of the absence of any such theoretical limit but also a lower cost of production. This report will review three state-of-the-art architectures for optical rectification developed by the leading groups worldwide. The review will compile a concise discussion on Metal-Double-Insulator-Metal diodes, CNT-Insulator-Metal diodes, and Point-contant-Metal-Insulator-Metal diodes, with an elaborative focus on their fabrication methods and results obtained.

Keywords: levelized cost of energy; rectenna; shockley-quiesser limit; metal-double-Insulator-metal diodes; CNT-insulator-metal diodes; point-contact-metal-insulator-metal diodes

1. Introduction

Nikolai Semyonovich Kardashev, an astronomer from the Soviet era, proposed a scale in 1964 to measure a civilization's technological advancement named the 'Kardishev Scale [2].' According to this hypothetical scale, a Type I civilization can access and store the planet's whole energy reservoir available, whereas Type II and Type III civilizations operate at solar and galactic energy levels. For Humanity to ascend towards finally becoming a Type I civilization, its members need to harness efficiently the most abundant energy source on Earth - the Sun. Our planet receives 170 W/m^2 power from our star, which is approximately 10^4 times the requirement for 10 billion people [3] (estimated population by the year 2050 [4]). Solar cells are the torchbearers for solar power harvesting, with crystalline Silicon photovoltaics (PVs) being the industry standard. A report by [5] documented a 1.045 TW power generation by solar cells in 2022, with an annual growth of approximately 22 % [6]. We require an increase in solar energy conversion of nearly 25 % or more inconsistently every year to achieve a Net Zero Scenario by 2030 [6]. This obligation puts immense pressure on researchers to keep improving the current PV technology concerning conversion efficiency and LCOE (Levelized Cost of Energy). Even with such exponential growth and rising popularity among scientists, the biggest roadblock in such a device is the Shockley-Quiesser limit, which states that single-junction solar cells cannot have a conversion efficiency of more than 33.7% [7]. One of the numerous ways of surpassing this limit is through technologies such as multi-junction solar cells [8,9], plasmon-assisted solar cells [10,11], and many other emerging PVs [12]. However, these novel designs are yet unsuitable for commercial use because of the high cost of production and maintenance and often the usage of toxic materials. Figure 3 shows the efficiency limits of solar cells over around 50 years.

 doi:10.20944/preprints202409.1932.v

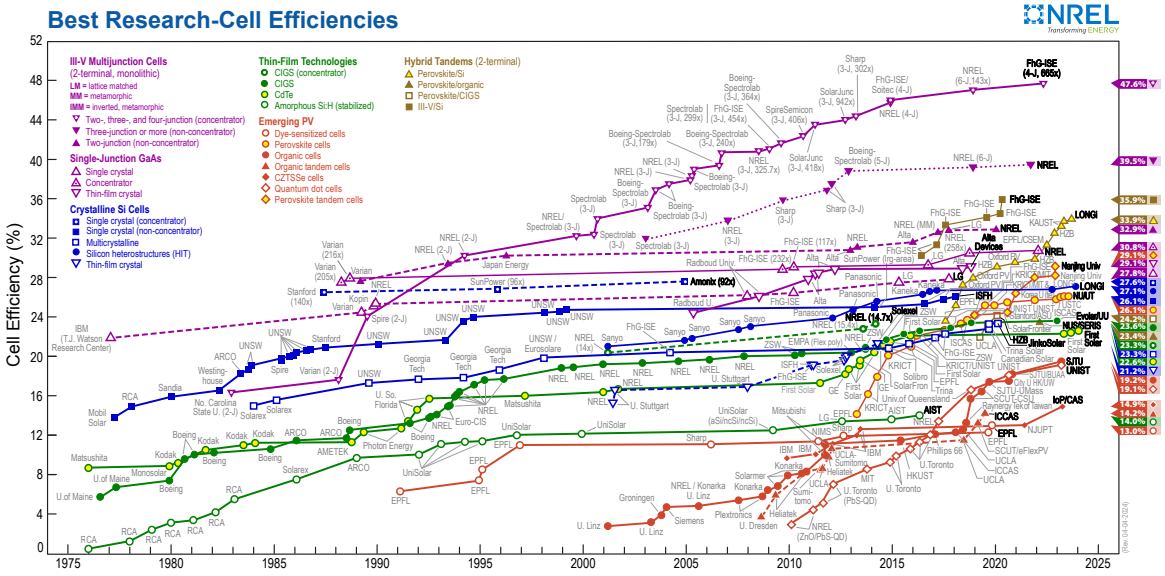

Figure 1. Efficiency limits of solar cells, reported by NREL [13].

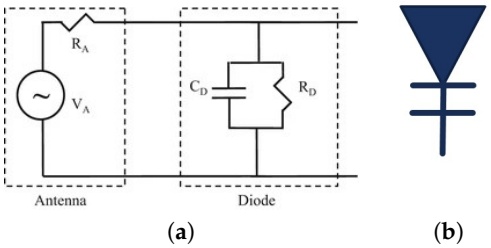

Figure 2. (**a**) A small signal equivalent circuit for rectenna [14], and (**b**) rectenna symbol.

Rectifying Antenna (or simply Rectenna) was first invented by William C Brown in 1964 and later patented in 1969 [15], just ten years after the first practical PV cell by the Bells lab [1]. The Rectenna-based energy harvesters have gained popularity within the last decade because of their numerous application within a broad frequency spectrum. Although the technology is yet to achieve a respectable efficiency in the THz regime due to current fabrication limits, rectennas are highly efficient at lower frequencies like GHz or MHz, reaching more than 88% power conversion [16]. Such low-frequency, low-power energy harvesters are highly suitable and efficient for biomedical applications [17,18]. One of the grandest applications the microwave rectennas have paved their way into is the Space-based Solar [19]. European Space Agency's SOLARIS [20] is the leading project in Space-based Solar, along with a few other private firms [21,22] attempting to achieve the Net-Zero Scenario.

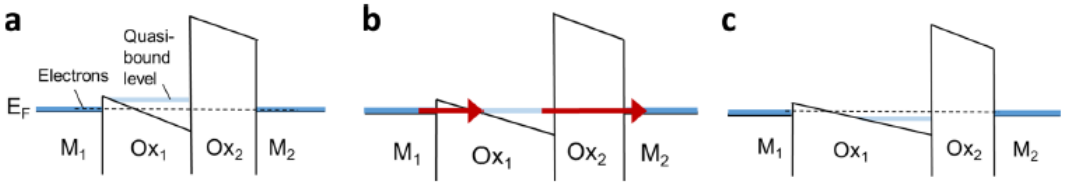

Figure 3. Energy-band diagrams of an MI2M structure with varying Ox1:Ox2 ratios. a 1:1, **b** 2:1, and **c** 3:1. The dashed line represents electron tunneling from the Fermi level of M1 to M2. In **a** and **c**, Fowler–Nordheim tunneling occurs through Ox1 and direct tunneling through Ox2. In **b**, electrons tunnel through the quasi-bound state present in the triangular quantum well, which enhances tunneling probability, increases current and responsivity, and decreases resistance. [23]

 doi:10.20944/preprints202409.1932.v

Among all the mentioned technologies, optical rectennas stand as the most promising contender in surpassing current solar energy harvesting methods. The presented report discusses the current state-of-the-art technologies in optical rectennas distinguished based on their different architectures by leading groups in this field.

2. Optical Rectennas

Rectenna consists of two parts—An antenna to collect and convert electromagnetic waves and a rectifying diode to rectify alternative current into direct current. Figure 4a shows an equivalent circuit for the rectenna system segregating the antenna and diode part and a symbol for the rectenna designed by the author in Figure 4b.

The overall efficiency of a rectenna device can be written in terms of stepwise efficiencies as follows [24]:

$$\eta = \eta_a \eta_s \eta_c \eta_j \tag{1}$$

Where η_a is the antenna efficiency, η_s is the efficiency of energy propagation from the antenna to the diode, η_c is the coupling efficiency between the antenna and diode, and lastly, η_j is the rectification efficiency of the diode. η_s can be omitted or taken as a unity by integrating the antenna within the diode. In the latest work by [25], η_a is achievable as high as 71.2 % for optical nanoantennas. Hence, to realize an efficient optical rectification, more emphasis is required on improving η_c and η_j.

3. Metal-Double-Insulator-Metal (MI^{2}M) Rectenna Diode [23]

In the current section, we focus on the first of the three rectification methods discussed in this work, i.e., the Metal-Insulator-Metal (MIM) diode. MIM diodes are highly suitable for high-frequency operations and go hand in hand with current CMOS fabrication methods, making them ideal for large-scale rectenna production. [23] presented the best work in this category, reporting the highest-ever coupling efficiency and overall conversion efficiency in MIM-based rectenna systems. The chosen structure is a Metal-Insulator-Insulator-Metal structure (MIIM) which offers enhanced current asymmetry and nonlinearity compared to a single-insulator MIM diode.

The most significant leap forward for rectenna technology in recent times came through this work which physically illustrated resonant tunneling in the MIM (or MI^{2}M) diodes at room temperature and low self-biasing voltage. Generally, the current responsivity in MIM diodes can be increased by thickening up the oxide layer, which also increases the resistance of the diode. But through the resonant tunneling effect, the authors could break off from this responsivity-resistance tradeoff, and the device demonstrated a high current responsivity of 0.52 A/W and 4kΩ at 4nm thickness of NiO. In the proposed Metal-Insulator-Insulator-Metal diode structure Nickel (M1) and Chromium (M2) are used as metal electrodes, whereas the NiO (Ox1) and Al_2O_3 (Ox2) are used as oxides layers, respectively. Moreover, a final gold layer is deposited on the top, assembling the whole structure as Ni/NiO/Al_2O_3/Cr/Au. Upon investigating different materials, the best results were achieved using work functions ϕ of 5 and 4.47 eV for Ni and Cr/Au respectively, and electron affinity χ values of 4.7 and 3.45 eV for NiO and Al_2O_3, respectively.

3.1. Fabrication

The shadow mask method, allowing a single self-aligned mask layer, which can resolve details as minuscule as 100 nm, is used for the device. The process begins with a Si substrate with 300 nm of thermally grown SiO_2 coating on top. The next step is the spin coating of polymethyl methacrylate (PMMA) in 4% anisol up to 260 nm thickness, followed by a 60 nm germanium layer evaporated on its top. Later, the pattern is etched over the germanium layer with a CF_4 etch (using ASML 5500 248 nm DUV stepper), and the PMMA layer is removed from underneath using high-pressure O_2 plasma etch, capable enough of undercutting Ge by 500 nm. After creating the desired pattern on the substrate,

 doi:10.20944/preprints202409.1932.v

metals, and insulators are sequentially deposited by thermal evaporation and sputtering. Nickel is the first metal layer evaporated till 35 nm at a 43° angle from right, followed by sputtering of oxide layers NiO (at different thicknesses) and Al_2O_3 (1 nm). The second metal layer is chosen to be 2.6 nm thick Chromium enclosed by 46 nm of Au layer.

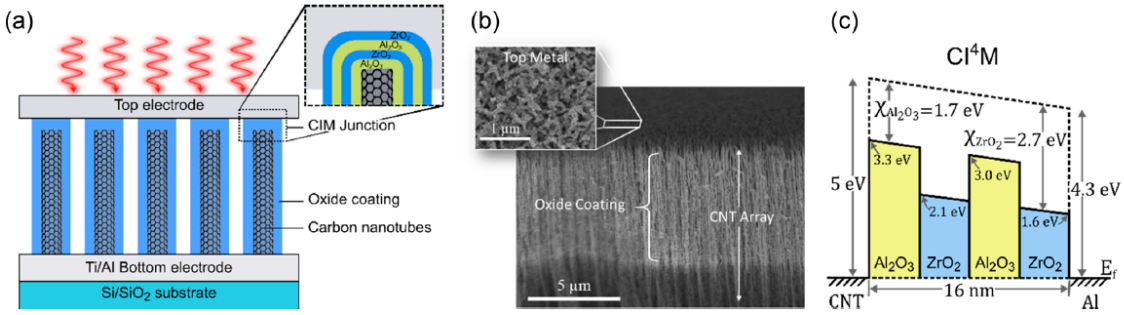

Figure 4. (**a**) Carbon nanotube rectenna device. (Inset) The tips of the CNTs are coated in a quad-insulator laminate of dielectric and capped with an Al top metal electrode to form a CNT/quad-insulator/metal (CI^4M) tunneling diode. (**b**) SEM side view of the CNT array coated with oxide and top metal. The oxide penetrates several microns into the array while conformally coating the CNTs. (Inset) The top metal coating in the array is not planar but rather forms an interdigitated network of metal-coated CNTs with gaps between. (**c**) Energy band diagram of the CI^4M structure featuring $Al_2O_3/ZrO2/Al_2O_3/ZrO2$ and an Al top electrode [26].

3.2. Results

The first oxide layer, Ox1, demonstrates the Fowler–Nordheim tunneling, and the second oxide layer, Ox2, the direct tunneling as the most dominant tunneling mechanism. Upon increasing the thickness of NiO, the current responsivity and resistance increase, but at an optimum value (4 nm), electrons start tunneling from M1 to M2 through quasi-bound states in the resonant well formed by oxide layers. This results in a drop in diode resistance. Figure 3 shows an illustration for a better understanding of the tunneling mechanism at different thickness ratios between Ox1 and Ox2.

The final Power Conversion Efficiency (PCE) is reported to be 17×10^{-9} % along with an open circuit voltage (V_{oc}) and short circuit current (I_{sc}) as 91.7 μV and 14.3 nA at 10.6 μm illumination wavelength respectively.

4. Carbon Nanotubes Optical Rectennas [26]

In this section, we proceed with another state-of-the-art optical rectenna architecture based on Carbon Nanotubes (CNTs) by [26]. CNTs make exemplary antenna elements, motivated by the extraordinary facility of CNTs to absorb electromagnetic energy in a broad spectrum [27–30] and the ability to be easily fabricated in vertically aligned arrays [31,32]. As the CNT nanoantennas operate at infrared and visible frequencies, light-matter interaction governs the conversion of optical waves into a localized electrical field through each antenna [27,33]. The optical rectification in CNT-based rectennas works similarly, if not exactly as in MIM diodes. The only difference is that CNT is the antenna and replaces one metal electrode making it a CNT-Insulator-Metal (CIM) diode. The current work reports a structure with four oxide layers consisting of alternating Al_2O_3 and ZrO_2 layers and an outer metal electrode of Al. The disparity between electron affinities ($\chi_{Al_2O_3} \simeq 1.7$ eV, $\chi_{ZrO_2} \simeq 2.7$ eV) [34–36] facilitates resonant or step tunneling mechanisms that alter electron conduction [37–39]. Improving step tunneling produces an enhanced forward current at a lower bias while suppressing the reverse bias current.

 doi:10.20944/preprints202409.1932.v

4.1. Fabrication

Multiwall carbon nanotubes were grown on SiO_2-coated Si. Ti/Al/Fe (100/10/3 nm) was deposited as the bottom electrode with Fe acting as the CNT catalyst. The vertical array of CNTs was grown using low-pressure chemical vapor deposition with C_2H_2 carbon source gas (Aixtron Black Magic). A growth time of around 180 s produces an array with heights around 10-30 μm, 8 nm diameter, and ~6 walls (Figure 4b). To expose the inner multi walls, the CNT tips were etched away with 30 s of O_2 plasma. The CNT array was then conformally coated with multiple oxide layers by atomic layer deposition at 250 °C. Layers were formed by cycling precursors of trimethylaluminum (for Al_2O_3) or tetrakis-(dimethylamine) zirconium (for ZrO_2) along with H_2O vapors. Extended purge times were used so precursors could infiltrate the CNT array, giving an average coating of 4 nm per 40 cycles. The top electrode metal was a 50 nm planar equivalent of Al deposited using thermal evaporation to minimize penetration through the oxide. A device area of 0.07 cm^2 was patterned with a shadow mask.

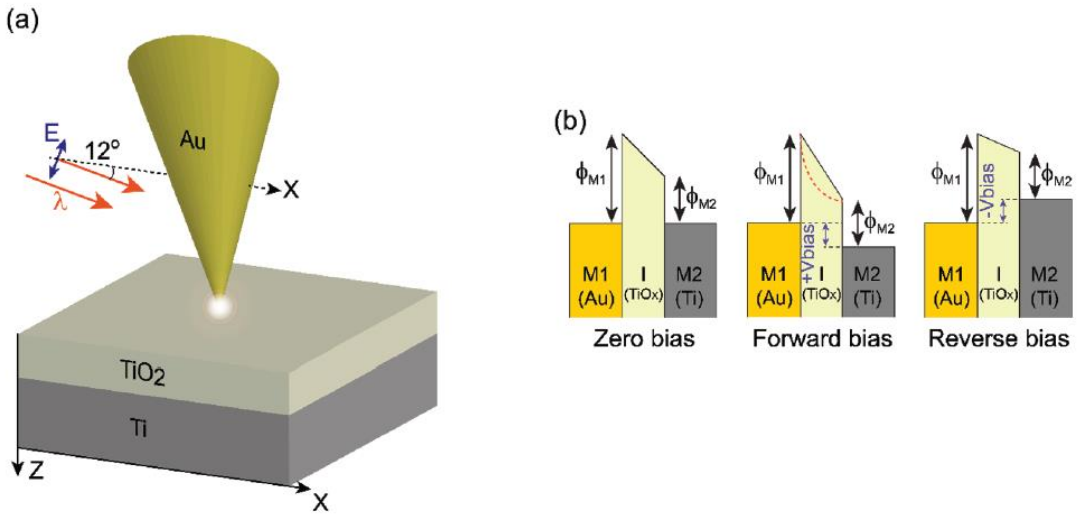

Figure 5. (**a**) Illustration of point contact MIM (pc-M1IM2) nano rectenna illuminated by an externally propagating collimated beam. (**b**) 1D energy diagram of an asymmetric MIM structure. M1 and M2 have work functions ϕ_{M1} and ϕ_{M2}, respectively. Under zero-bias conditions, all Fermi levels are aligned. Applying a positive bias to M2 leads to a forward bias situation where electrons near the Fermi level flow from M1 to M2. Applying a negative bias to M2 leads to a reverse bias situation where electrons flow from M2 to M1. The dashed red curve highlighted for the forward bias situation manifests the energy diagram change occurring in the point contact configuration [40].

4.2. Results

The proposed CI^4M device demonstrates exceptional diode properties suitable for optical rectification: asymmetry surpassing 300 and high nonlinearity beginning at a low turn-on voltage of ~0.3 V. Peak responsivity reported is 6 A/W. Moreover, with four dielectric layers, the diode experiences additional step tunneling in either direction, which is an introspection from an abrupt increase in reverse bias current at -1 V. Resonant tunneling is also suspected in the proposed device because of a quantum well forming within the shallow inner ZrO_2 layer (layer #2) sandwiched between layers of Al_2O_3. Since the diode is not stable past $\pm$3 V, the dominant conduction mechanism at a higher basis is still unclear.

The CNTs rectenna diode is illuminated with 5 mW/cm^2 incident laser power over a wavelength range of 404-980 nm. For the wavelengths tested, the maximum performance occurring at 638 nm: the open-circuit voltage is V_{oc} = -95 mV, and the short-circuit current is I_{sc} = 7.6 nA/cm^2 (or 0.532 nA); with respect to incident intensity total PCE, which equals 3×10^{-6}% at the maximum power point

 doi:10.20944/preprints202409.1932.v

(MPP). Despite a low efficiency because of the large resistance associated with the 16 nm thick insulator that is chosen to maximize asymmetry, device stability, and breakdown voltage for this study, a high voltage responsivity of 250 V/W is observed for a 0.07 cm^2 device, making it a potential candidate for detectors.

5. Point-Contact-Insulator-Metal Rectenna Diode [40]

Now we will discuss our final and most efficient rectenna architecture to date. The device proposed by [40] is a Point-Contact-Insulator-Metal rectenna diode that works similarly to a point-contact diode, which is very suitable for high-frequency operations. In our previous discussions, the current asymmetry was achieved from a material point-of-view by choosing oxide layers of appropriate work functions and thicknesses. Whereas, in the proposed architecture, the asymmetry is conceived both from a geometrical [41,42] and material [43] point of view (see Figure 5a and b, respectively). The nano rectenna is defined by a point-contact Metal-Insulator-Metal tunneling diode (hereafter pc-MIM), where the pc-M1 component also acts as a receiving plasmonic nano-antenna. In particular, authors considered an Au-coated nanocone (pc-M1) and a flat 50 nm thick Ti substrate (M2) as the nano rectenna electrodes due to the significant difference in their work functions ϕ, [44] with ϕ_{M1} = 5.10 eV and ϕ_{M2} = 4.33 eV, respectively (see Figure 5b).

5.1. Fabrication

The nanocone antenna was fabricated on top of an atomic force microscope (AFM) cantilever using FIB milling (FEI Nanolab 600 dual beam) with a Ga ion beam. A contact mode silicon AFM cantilever probe (MikroMasch CSC38-Al) with a long cone/pyramid was chosen as the platform for the nanocone fabrication (lever length 350 μm, lever thickness 1 μm, and probe height 15 μm). In particular, the Si cantilever probe was coated with a 7 nm Ti layer to increase its adhesion capability. It was followed by a further coating of 15 nm of Au to create a uniform conductive layer. Afterward, the AFM tip was etched, creating a plateau where a Pt-C nanocone was grown via the GIS system. Importantly, this approach could guarantee the realization of a Pt-C nanocone with a ≈10 nm apex radius with extremely high reproducibility. An over-layer of ≈20 nm of Au, thick enough to support SPPs, was then deposited via Ar ion sputter on the structure, followed by 20 min of annealing process at 195 °C characterized by a fast heating ramp and a slowly decaying cooling ramp. This final procedure was set to smooth as much as possible the nanocone surface, a necessary condition for improved electric contact with the underneath substrate.

5.2. Results

In the proposed nano rectenna architecture, two main mechanisms can contribute to the current flowing from M1 to M2 in the pc-MIM structure: i) direct tunneling, namely, HEs tunneling through the barrier with a width equal to the thickness of the insulator, and ii) Fowler Nordheim (FN) tunneling, where HEs tunnel through the triangular shaped tilted barrier with a width smaller than the insulator thickness. Both the direct and Fowler-Nordheim mechanisms benefit from forming a plasmonic resonance on the nanocone.

The device is illuminated with two different laser sources of wavelengths λ=1064 nm (intensity = 12.95 MW/m^2) and λ=780 nm (intensity = 7.10 MW/m^2) at an incident angle of 12° with respect to the X axis (the angle of incidence dearly affects the photocurrent). The best results are obtained for a 1064 nm laser, with total PCE as 2.3×10^{-4}%, with the open-circuit voltage is V_{oc} = -151.5 mV, and the short-circuit current is I_{sc} = 23.5 pA.

6. Conclusions

In the presented report, we reviewed three state-of-the-art rectenna technologies contributing toward alternative solar energy harvesting methods and other high-frequency applications. The discussion started with the Metal-double-Insulator-Metal (MIIM) rectenna diode, which offers the least

 doi:10.20944/preprints202409.1932.v

efficiency, yet is the most promising among all three in realizing rectenna application at a commercial level. The MIIM rectenna diodes are highly compatible with mass-scale CMOS fabrication methods such as nano transfer printing [45]. Later we move with a different architecture, yet not so distinctive from MIIM diodes: Carbon Nanotubes rectenna diodes, or to be precise, CNTs-quad-Insulator-Metal diode (CI^4M). Not only the CI^4M rectenna diodes have shown a better efficiency from MIIM but also a broader frequency spectrum in visible and IR amongst all three architectures. However, the current knowledge of CNT antennas is still based on classical dipole antenna theory and offers limitations in operation near CNT plasmon frequencies. Moreover, the disorder and non-uniform lengths of CNTs deteriorate their antenna behavior over large areas. Lastly, we shifted our focus to the most efficient rectenna device to date: Point-contant-Insulator-Metal (pc-MIM) rectenna diode. Even though pc-MIM is closest to becoming practical in the coming future compared to MIIM and CI^4M, the significant drawbacks with such devices are their lack of scalability and high dependence on the angle of incidence, making them least suitable for a practical solar cell alternative at the moment. Table 1 tabulates all the results reposted by authors of these respective devices.

But will the rectenna solar cells ever be possible? For the last six decades, ever since the invention of the first-ever rectenna [15], this question has been asked by experts and young researchers. In fact, the purpose of this review report is to ask this question time and again but also to understand significant advances within just the last decade. As long as this question is kept being asked, the progression will never cease.

Table 1. Total Power Conversion Efficiency, Open Circuit Voltage, V_{oc}, and Short Circuit Current, I_{sc} at the wavelength of optimum operation, reported by [23,26] and [40].

	MIIM [23]	CI^4M [26]	pc-MIM [40]
Wavelength of optimum operation (nm)	10600	638	1064
Total Power Conversion Efficiency (%)	17×10^{-9}	3×10^{-6}	2.3×10^{-4}
Open Circuit Voltage, V_{oc} (mV)	0.0917	-95	-151.5
Short Circuit Current, I_{sc} (nA)	14.3	0.532	0.0235

References

1. First Photovoltaics.
2. Kardashev, N.S. Transmission of Information by Extraterrestrial Civilizations. 1964.
3. Chandler, D.L. Shining brightly.
4. Population.
5.
6. Iea. Solar PV – analysis.
7. Shockley, W.; Queisser, H.J. Detailed Balance Limit of Efficiency of p-n Junction Solar Cells, 1961. doi:10.1063/1.1736034.
8. Dimroth, F.; Kurtz, S. High-Efficiency Multijunction Solar Cells. *MRS Bulletin* **2007**, *32*, 230–235. doi:10.1557/mrs2007.27.
9. Geisz, J.F.; France, R.M.; Schulte, K.L.; Steiner, M.A.; Norman, A.G.; Guthrey, H.L.; Young, M.R.; Song, T.; Moriarty, T. Six-junction III–V solar cells with 47.1% conversion efficiency under 143 Suns concentration, 2020. doi:10.1038/s41560-020-0598-5.
10. Ding, B.; Lee, B.J.; Yang, M.; Jung, H.S.; Lee, J.K. Surface-Plasmon Assisted Energy Conversion in Dye-Sensitized Solar Cells, 2011. doi:10.1002/aenm.201000080.
11. Jang, Y.H.; Jang, Y.J.; Kim, S.; Quan, L.N.; Chung, K.; Kim, D.H. Plasmonic solar cells: from rational design to mechanism overview. *Chemical reviews* **2016**, *116*, 14982–15034.
12. Almora, O.; Baran, D.; Bazan, G.C.; Berger, C.; Cabrera, C.I.; Catchpole, K.R.; Erten-Ela, S.; Guo, F.; Hauch, J.; Ho-Baillie, A.W.Y.; Jacobsson, T.J.; Janssen, R.A.J.; Kirchartz, T.; Kopidakis, N.; Li, Y.; Loi, M.A.; Lunt, R.R.;

 doi:10.20944/preprints202409.1932.v

Mathew, X.; McGehee, M.D.; Min, J.; Mitzi, D.B.; Nazeeruddin, M.K.; Nelson, J.; Nogueira, A.F.; Paetzold, U.W.; Park, N.; Rand, B.P.; Rau, U.; Snaith, H.J.; Unger, E.; Vaillant-Roca, L.; Yip, H.; Brabec, C.J. Device Performance of Emerging Photovoltaic Materials (Version 1), 2020. doi:10.1002/aenm.202002774.

13.

14. Grover, S.; Moddel, G. Applicability of Metal/Insulator/Metal (MIM) Diodes to Solar Rectennas. *IEEE Journal of Photovoltaics* **2011**, *1*, 78–83. doi:10.1109/JPHOTOV.2011.2160489.
15. Brown, W.C. Microwave to dc converter, 1969.
16. Pandey, R.; Shankhwar, A.K.; Singh, A. AN IMPROVED CONVERSION EFFICIENCY OF 1.975 TO 4.744 GHZ RECTENNA FOR WIRELESS SENSOR APPLICATIONS, 2021. doi:10.2528/pierc20121102.
17. Ding, S.; Koulouridis, S.; Pichon, L. Implantable rectenna system for biomedical wireless applications, 2019. doi:10.1109/wptc45513.2019.9055687.
18. Ojha, S.S.; Singhal, P.; Thakare, V.V. Dual-band rectenna system for biomedical wireless applications, 2022. doi:10.1016/j.measen.2022.100532.
19. Space solar power - national space society, 2022.
20. Solaris.
21. Space solar, developing and commercialize space-based solar power, 2023.
22.
23. Belkadi, A.; Weerakkody, A.; Moddel, G. Demonstration of resonant tunneling effects in metal-double-insulator-metal (MI2M) diodes, 2021. doi:10.1038/s41467-021-23182-0.
24. Grover, S.; Moddel, G. Optical Frequency Rectification, 2013. doi:10.1007/978-1-4614-3716-1_2.
25. Midrio, M.; Pierantoni, L.; Boscolo, S.; Truccolo, D.; Mencarelli, D. Nano-antenna array for high efficiency sunlight harvesting, 2022. doi:10.1364/oe.450020.
26. Anderson, E.C.; Cola, B.A. Photon-Assisted Tunneling in Carbon Nanotube Optical Rectennas: Characterization and Modeling, 2019. doi:10.1021/acsaelm.9b00058.
27. He, X.; Fujimura, N.; Lloyd, J.M.; Erickson, K.J.; Talin, A.A.; Zhang, Q.; Gao, W.; Jiang, Q.; Kawano, Y.; Hauge, R.H. Carbon Nanotube Terahertz Detector. *Nano Lett.* **2014**, *14*, 3953.
28. Zhang, T.F.; Li, Z.P.; Wang, J.Z.; Kong, W.Y.; Wu, G.A.; Zheng, Y.Z.; Zhao, Y.W.; Yao, E.X.; Zhuang, N.X.; Luo, L.B. Broadband Photodetector Based on Carbon Nanotube Thin Film/Single Layer Graphene Schottky Junction. *Sci. Rep.* **2016**, *6*, 38569.
29. Kumar, S.; Nehra, M.; Kedia, D.; Dilbaghi, N.; Tankeshwar, K.; Kim, K.H. Carbon Nanotubes: A Potential Material for Energy Conversion and Storage. *Prog. Energy Combust. Sci.* **2018**, *64*, 219.
30. Ren, L.; Zhang, Q.; Pint, C.L.; Wójcik, A.K.; Bunney, M.; Arikawa, T.; Kawayama, I.; Tonouchi, M.; Hauge, R.H.; Belyanin, A.A. Collective Antenna Effects in the Terahertz and Infrared Response of Highly Aligned Carbon Nanotube Arrays. *Phys. Rev. B: Condens. Matter Mater. Phys.* **2013**, *87*, 161401.
31. Choi, W.B.; Bae, E.; Kang, D.; Chae, S.; Cheong, B.; Ko, J.; Lee, E.; Park, W. Aligned Carbon Nanotubes for Nanoelectronics. *Nanotechnology* **2004**, *15*, S512.
32. Jakubinek, M.B.; White, M.A.; Li, G.; Jayasinghe, C.; Cho, W.; Schulz, M.J.; Shanov, V. Thermal and Electrical Conductivity of Tall, Vertically Aligned Carbon Nanotube Arrays. *Carbon* **2010**, *48*, 3947.
33. Olmon, R.L.; Raschke, M.B. Antenna-Load Interactions at Optical Frequencies: Impedance Matching to Quantum Systems. *Nanotechnology* **2012**, *23*, 444001.
34. Alimardani, N.; Conley, J.F. Enhancing Metal-Insulator-Insulator-Metal Tunnel Diodes via Defect Enhanced Direct Tunneling. *Appl. Phys. Lett.* **2014**, *105*, 082902.
35. Alimardani, N.; King, S.W.; French, B.L.; Tan, C.; Lampert, B.P.; Conley, J.F. Investigation of the Impact of Insulator Material on the Performance of Dissimilar Electrode Metal-Insulator-Metal Diodes. *J. Appl. Phys.* **2014**, *116*, 024508.
36. Kukli, K.; Kemell, M.; Vehkamäki, M.; Heikkilä, M.J.; Mizohata, K.; Kalam, K.; Ritala, M.; Leskelä, M.; Kundrata, I.; Fröhlich, K. Atomic Layer Deposition and Properties of Mixed Ta 2 O 5 and ZrO 2 Films. *AIP Adv.* **2017**, *7*, 025001.
37. Alimardani, N.; Conley, J.F. Step Tunneling Enhanced Asymmetry in Asymmetric Electrode Metal-Insulator-Insulator-Metal Tunnel Diodes. *Appl. Phys. Lett.* **2013**, *102*, 143501.
38. Singh, A.; Ratnadurai, R.; Kumar, R.; Krishnan, S.; Emirov, Y.; Bhansali, S. Fabrication and Current-Voltage Characteristics of NiOx/ZnO Based MIIM Tunnel Diode. *Appl. Surf. Sci.* **2015**, *334*, 197.

39. Weerakkody, A.D.; Sedghi, N.; Mitrovic, I.Z.; Van Zalinge, H.; Nemr Noureddine, I.; Hall, S.; Wrench, J.S.; Chalker, P.R.; Phillips, L.J.; Treharne, R. Enhanced Low Voltage Nonlinearity in Resonant Tunneling Metal-Insulator-Insulator-Metal Nanostructures. *Microelectron. Eng.* **2015**, *147*, 298.
40. Mupparapu, R.; Cunha, J.; Tantussi, F.; Jacassi, A.; Summerer, L.; Patrini, M.; Giugni, A.; Maserati, L.; Alabastri, A.; Garoli, D.; Proietti Zaccaria, R. High-Frequency Light Rectification by Nanoscale Plasmonic Conical Antenna in Point-Contact-Insulator-Metal Architecture, 2022. doi:10.1002/aenm.202103785.
41. Mayer, A.; Chung, M.S.; Lerner, P.B.; Weiss, B.L.; Miskovsky, N.M.; Cutler, P.H. Classical and quantum responsivities of geometrically asymmetric metal-vacuum-metal junctions used for the rectification of infrared and optical radiations, 2011. doi:10.1116/1.3599756.
42. Mayer, A.; Chung, M.S.; Weiss, B.L.; Miskovsky, N.M.; Cutler, P.H. Simulations of infrared and optical rectification by geometrically asymmetric metal–vacuum–metal junctions for applications in energy conversion devices, 2010. doi:10.1088/0957-4484/21/14/145204.
43. Moddel, G.; Weerakkody, A.; Doroski, D.; Bartusiak, D. Optical-Cavity-Induced Current, 2021. doi:10.3390/sym13030517.
44. Jayaswal, G.; Belkadi, A.; Meredov, A.; Pelz, B.; Moddel, G.; Shamim, A. Optical rectification through an Al2O3 based MIM passive rectenna at 28.3 THz, 2018. doi:10.1016/j.mtener.2017.11.002.
45. Bareiß, M.; Kälblein, D.; Krenz, P.M.; Zschieschang, U.; Klauk, H.; Scarpa, G.; Fabel, B.; Porod, W.; Lugli, P. Large-Area Fabrication of Antennas and Nanodiodes, 2013. doi:10.1007/978-1-4614-3716-1_14.